Exp Fluids
DOI 10.1007/s00348-006-0233-7

RESEARCH ARTICLE

Intensity Capping: a simple method to improve cross-correlation PIV results

Uri Shavit · Ryan J. Lowe · Jonah V. Steinbuck

Received: 2 September 2006 / Revised: 23 October 2006 / Accepted: 24 October 2006

Abstract A common source of error in particle image velocimetry (PIV) is the presence of bright spots within the images. These bright spots are characterized by grayscale intensities much greater than the mean intensity of the image and are typically generated by intense scattering from seed particles. The displacement of bright spots can dominate the cross-correlation calculation within an interrogation window, and may thereby bias the resulting velocity vector. An efficient and easy-to-implement image-enhancement procedure is described to improve PIV results when bright spots are present. The procedure, called Intensity Capping, imposes a user-specified upper limit to the grayscale intensity of the images. The displacement calculation then better represents the displacement of *all* particles in an interrogation window and the bias due to bright spots is reduced. Four PIV codes and a large set of experimental and simulated images were used to evaluate the performance of Intensity Capping. The results indicate that Intensity Capping can significantly increase the number of valid vectors from experimental image pairs and reduce displacement error in the analysis of simulated images. A comparison with other PIV image-enhancement techniques shows that Intensity Capping offers competitive performance, low computational cost, ease of implementation, and minimal modification to the images.

U. Shavit (✉)
Civil and Environmental Engineering, Technion,
Haifa 32000, Israel
e-mail: aguri@technion.ac.il

R. J. Lowe · J. V. Steinbuck
Environmental Fluid Mechanics Laboratory,
Stanford University, Stanford, CA 94305, USA

1 Introduction

A common problem in particle image velocimetry (PIV) studies is the appearance of bright spots in the images. The grayscale intensity of these bright spots is typically much higher than the mean intensity of the images. Bright spots may result from coalesced particles, overlapping particles within the field of view, or individual particles located within highly illuminated regions (e.g., midway through the laser light sheet). In addition, many CCD cameras used in PIV experiments suffer from pixel anomalies (e.g., charge leakage), which may increase the intensity and total area of bright spots in an image.

Most PIV codes use the cross-correlation function to compute the particle displacements. The advantage of cross-correlation PIV over other methods, such as particle tracking velocimetry (PTV), is the relatively large sample size (number of particle pairs) that is used to calculate each velocity vector. A large number of particle pairs can increase the strength of the correlation peak, improving the detection of the peak and reducing the uncertainty in the displacement calculation (Raffel et al. 1998). For example, Keane and Adrian (1992) found that cross-correlation PIV requires more than five particle pairs within the interrogation window to yield a valid vector detection probability higher than 95%. However, if bright spots

are present in the images, the cross-correlation may be dominated by a small number of high-intensity pixels. As a result, the number of particle pairs that contribute to the cross-correlation peak may be small (<5). Furthermore, if the displacement of the bright spots differs from the mean particle displacement within a subwindow (e.g., in sheared or turbulent flows), then the resulting velocity vector may be spurious.

A common approach for removing spurious vectors is to employ filtering techniques after the cross-correlation analysis. The rejected vectors are then replaced using interpolation based on kernel weight functions, typically of 8 or 24 neighboring vectors. Since filtering techniques may not detect all of the spurious vectors and since interpolation introduces unknown errors, it is desirable to minimize the generation of spurious vectors.

In order to minimize the occurrence of spurious vectors in PIV results, two approaches are often implemented: PIV algorithm improvement and image enhancement prior to PIV processing. The symmetric phase only filtering (SPOF) technique is an example of PIV algorithm improvement (Wernet 2005). This technique modifies the FFT procedure by adding a normalized filter such that only the phase contributes to the cross-correlation result. Image-enhancement techniques, such as the one presented in this paper, do not necessitate modifications to the PIV algorithm since they are applied prior to PIV processing. Westerweel (1993) proposed a min/max image-enhancement technique that minimizes variations in the recorded particle image intensities and reduces background noise. Dellenback et al. (2000) modified their low quality PIV images by applying enhancement techniques such as thresholding, contrast enhancement, histogram equalization, and histogram hyperbolization. Roth and Katz (2001) developed a modified histogram equalization (MHE) technique that combines thresholding and histogram stretching. Fore et al. (2005) enhanced their PIV images by subtracting a background image (obtained by averaging a series of images) and then linearly stretching the grayscale range. Notably, each of these techniques fully re-maps the images by replacing the original intensity of each pixel with a new value. Thus, care must be taken to avoid image modifications that degrade the accuracy of the PIV results.

In this paper, we provide an image-enhancement procedure for improving PIV results when bright spots are present in the images. The procedure only affects a small number of pixels in the images and thereby limits potentially harmful image modifications. The improvement is achieved by applying an upper limit to the grayscale values of the images. This image enhancement, called Intensity Capping, is performed before the image pair is analyzed using the cross-correlation. As such, it can be applied when using either commercial or open-source PIV codes. Being a simple modification to the images, Intensity Capping is computationally cheap and easy to implement.

2 Methodology

2.1 Description of Intensity Capping

To explain Intensity Capping, we examine an interrogation window containing particles that move a distance $\mathrm{d}\boldsymbol{x}$ between subsequent images. The first grayscale image is described by f and the second is described by g. The two-dimensional cross-correlation of the images is given by

$$\phi_{fg}(\boldsymbol{m}) = \int f(\boldsymbol{x}' + \boldsymbol{m}) g(\boldsymbol{x}') \mathrm{d}\boldsymbol{x}', \tag{1}$$

where $\boldsymbol{x}'$ is the spatial variable, $\boldsymbol{m}$ is the shift in the correlation plane, and bold indicates two-dimensional variables. The limits of integration will depend on the size of the interrogation window. The two-dimensional particle displacement, $\mathrm{d}\boldsymbol{x}$, is identified by the spatial location of the cross-correlation maximum:

$$\phi_{fg}(\mathrm{d}\boldsymbol{x}) = \max(\phi_{fg}(\boldsymbol{m})). \tag{2}$$

Suppose now that the first and second images, f and g, contain bright spots with intensities that are much greater than the mean intensity of the images. We decompose image f as $f = f_1 + f_2$ and image g as $g = g_1 + g_2$, where the subscript "1" indicates the image without the bright spots and the subscript "2" indicates the imaged bright spots. Substituting these decomposed forms for f and g into Eq. 1 gives

$$\phi_{fg}(\boldsymbol{m}) = \phi_{f1g1}(\boldsymbol{m}) + \phi_{f1g2}(\boldsymbol{m}) + \phi_{f2g1}(\boldsymbol{m}) + \phi_{f2g2}(\boldsymbol{m}), \tag{3}$$

where

$$\phi_{f1g1}(\boldsymbol{m}) = \int f_1(\boldsymbol{x}' + \boldsymbol{m}) g_1(\boldsymbol{x}') \mathrm{d}\boldsymbol{x}', \tag{4a}$$

$$\phi_{f1g2}(\boldsymbol{m}) = \int f_1(\boldsymbol{x}' + \boldsymbol{m}) g_2(\boldsymbol{x}') \mathrm{d}\boldsymbol{x}', \tag{4b}$$

$$\phi_{f2g1}(\boldsymbol{m}) = \int f_2(\boldsymbol{x}' + \boldsymbol{m}) g_1(\boldsymbol{x}') \mathrm{d}\boldsymbol{x}', \tag{4c}$$

$$\phi_{f2g2}(\boldsymbol{m}) = \int f_2(\boldsymbol{x}' + \boldsymbol{m}) g_2(\boldsymbol{x}') \mathrm{d}\boldsymbol{x}'. \quad (4\mathrm{d})$$

Finally, substitution of Eq. 3 into Eq. 2 yields the equation for the particle displacement,

$$\phi_{f_g}(\mathrm{d}\boldsymbol{x}) = \max\Big(\phi_{f1g1}(\boldsymbol{m}) + \phi_{f1g2}(\boldsymbol{m}) + \phi_{f2g1}(\boldsymbol{m}) + \phi_{f2g2}(\boldsymbol{m})\Big) \quad (5)$$

Assuming the number of bright spots in the interrogation window is small, $\phi_{f1g1}(\boldsymbol{m})$ represents the contribution of the majority of the particles to the total cross-correlation, ϕ_{fg} $(\boldsymbol{m})$. The remaining three terms, ϕ_{f1g2} $(\boldsymbol{m})$ $\phi_{f2g1}(\boldsymbol{m})$ and $\phi_{f2g2}(\boldsymbol{m})$, represent the contribution to the cross-correlation by the small number of bright spots. Note that the bright spots correlate both with themselves and with the particles of moderate intensity. Since the intensities of f_2 and g_2 are high, the contribution to the correlation by bright spots can be significant, if not dominant. The calculated displacement may then depend on the correlations of the bright spots. If the bright spots do not follow the local flow then ϕ_{fg} $(\boldsymbol{m})$ may be biased and spurious vectors may result.

To ameliorate this problem, we propose to impose an upper limit on the grayscale values of all the pixels in images f and g. As illustrated in Fig. 1, the upper limit can be expressed as $I_0 + n{\cdot}\sigma_I$, where I_0 is the grayscale median intensity of the image, σ_I is the standard deviation of the intensity, and n is a user-specified constant (e.g., $n = 2$ in Fig. 1). Pixels with grayscale intensities higher than $I_0 + n{\cdot}\sigma_I$ are replaced by this grayscale value (i.e., the value $I_0 + n{\cdot}\sigma_I$); all of the other pixels are left unchanged. As a result of this Intensity Capping, the intensity values in f_2 and g_2 are reduced substantially and the contributions of ϕ_{f1g2} $(\boldsymbol{m})$, ϕ_{f2g1} $(\boldsymbol{m})$, and ϕ_{f2g2} $(\boldsymbol{m})$ to ϕ_{fg} $(\boldsymbol{m})$ are diminished. Consequently, the calculated displacement, $\mathrm{d}\boldsymbol{x}$, in Eq. 5 will better reflect the average displacement of *all* particles in the interrogation window and will be less biased towards the displacement of bright spots.

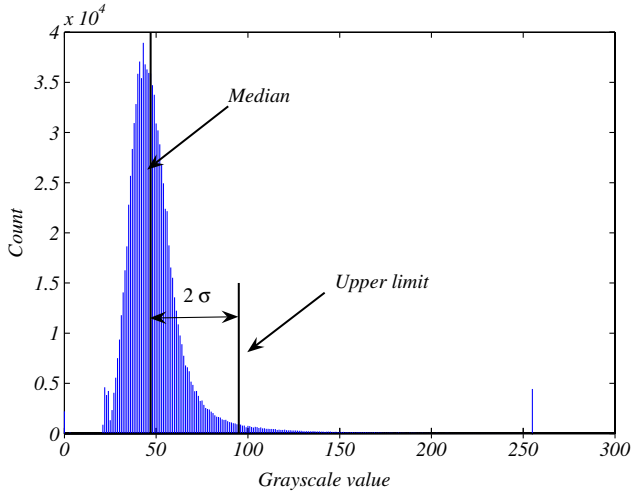

Fig. 1 An intensity histogram for image "Flume_1" (8-bit), its grayscale median, and an example of an upper limit ($I_0 + 2{\cdot}\sigma_I$) used for Intensity Capping. Note the group of saturated pixels with a value of 255

2.2 Application of Intensity Capping to PIV images

The performance of Intensity Capping is evaluated for both experimental images (Sect. 3) and synthetic images (Sect. 4). Capped image pairs were processed using four different cross-correlation PIV codes: MatPIV 1.6.1 (Sveen 2004); UraPIV (Gurka et al. 1999); VidPIV 4.0 g (ILA, Juelich, Germany, 2001); and Insight 6.0 (TSI, Shoreview, MN, 2005). The first two codes were developed using Matlab (Mathworks) and are open-source. The second two codes are commercially distributed. We emphasize that we do not seek to compare the effectiveness of these PIV codes, but rather seek to evaluate the performance of Intensity Capping for a broad set of PIV algorithms.

In all of the PIV analysis, interrogation windows of 32×32 pixels with 50% overlap were used, yielding velocity vectors every 16 pixels. When using UraPIV, VidPIV, and Insight, only a single cross-correlation pass (iteration) was performed. However, a multiple-pass algorithm was implemented when using MatPIV. In the first pass, an interrogation window of 64×64 pixels was used to calculate the particle displacements. The displacement results were then used to locate the center of the interrogation window in the second pass. Two more passes, using 32×32 pixel windows, were used to generate the final velocity vector maps.

In Sect. 3, the performance of Intensity Capping is analyzed using a set of experimental images. For each image pair, intensity capped images were generated by assigning pixels with an intensity exceeding $I_0 + n{\cdot}\sigma_I$, with the value $I_0 + n{\cdot}\sigma_I$. In order to identify the value of n that yielded the greatest improvement to the PIV results, Intensity Capping was applied for a range of different n values (i.e., –0.1 to either 11 or 40, depending on the image pair). For these experimental image pairs, the true velocity field is not known. Therefore, in order to assess the effect of Intensity Capping, a local consistency filter was used to quantify the change in the number of valid vectors. Those velocity vectors (u and v) within two standard deviations of the median of their 24 ($=5^2-1$) neighbors were

considered valid, while those outside this range were marked as outliers. This filter range appeared appropriate for the velocity maps considered here. It is important to emphasize that the number of valid vectors can be a function of both the performance of the PIV codes and the quality of the images. Thus, in order to evaluate Intensity Capping, we are strictly interested in the relative improvement (i.e., reduction of spurious vectors) obtained by each code for each individual experiment.

In Sect. 4, a series of synthetic images are used to evaluate the performance of Intensity Capping for various flow conditions (turbulence, shear, and cross-plane motion) and image characteristics (particle seeding density and peak particle intensity). These images were capped either at specific intensity values (ranging from 1 to 3,500) or by using the same procedure as applied for the experimental images. Using synthetic images, it is possible to directly quantify the effect the Intensity Capping by comparing capped PIV results to the known, true velocity field. In the evaluation of the synthetic image trials, only MatPIV was used for the PIV processing.

2.3 Comparison with other image-enhancement techniques

In Sects. 3 and 4, results obtained by Intensity Capping are compared to three alternative image-enhancement algorithms. The first image-enhancement technique considered is MHE (Roth and Katz 2001). MHE was implemented as described by Roth and Katz (2001), with the exception that the entire image was used as a single tile. This change had little effect on the MHE results since the images do not suffer from reflections from solid surfaces and their illumination is relatively uniform. This technique involves varying a parameter, x, which describes the percent area of the image that does not contain particles. The MHE algorithm was applied to each image pair using a range of different x values. The velocity field corresponding to the value of x giving the least number of spurious vectors was then selected for comparison with Intensity Capping.

The second image-enhancement algorithm considered is the min/max technique (Westerweel 1993). In this procedure, the grayscale value of each pixel is modified as follows,

$$I_{\mathrm{m}}(x,y) = I_{\max}\left(\frac{I(x,y) - \min(I_{\mathrm{tile}})}{\max(I_{\mathrm{tile}}) - \min(I_{\mathrm{tile}})}\right), \tag{6}$$

where I_{m} (x,y) is the new, modified grayscale value of pixel (x,y), $I(x,y)$ is the original grayscale value of pixel (x,y), $I_{\max}$ is the maximum possible image intensity (e.g., 255 for 8-bit images and 4,095 for 12-bit images) and I_{tile} is the intensity array of user-specified size, centered about pixel (x,y). Following Westerweel (1993), we first computed the minimum and maximum values of I_{tile} over the entire image and then applied a uniform, moving-average filter with a template size equal to the tile size to generate the values of $\min(I_{\mathrm{tile}})$ and $\max(I_{\mathrm{tile}})$. To avoid a nearly zero denominator in Eq. 6, we did not apply min/max for the condition $\max(I_{\mathrm{tile}}) - \min(I_{\mathrm{tile}}) < 10$. The optimum tile size depends on characteristics of the image pair, including particle image size and spatial variations in the image background. For this study we evaluated the min/max technique for a range of tile sizes: 5×5, 9×9, 15×15 and 25×25 pixels.

The final image-enhancement algorithm used for comparison is contrast limited adaptive histogram equalization (CLAHE), as implemented using 'adapthisteq.m' in the Matlab Image Processing Toolbox, Mathworks, Inc. The CLAHE function was applied using the default setting (full grayscale range of the original images, tiles of 8×8 pixels, and a uniform histogram shape) with no further tuning.

3 Evaluation of experimental PIV images

3.1 Experimental images

Six experimental image pairs were evaluated (Table 1). "Flume_1" (Rosenzweig 2005), "Wave_1" (Shavit et al. 2003), and "Air" (Gurka 1999) were obtained at the Technion (Israel Institute of Technology, Haifa, Israel). "Ocean" was obtained by the Marine Physical Laboratory, Scripps Institution of Oceanography, University of California, San Diego. "Flume_2" and "Wave_2" (Lowe 2005) were obtained at the Environmental Fluid Mechanics Laboratory, Stanford University. These six image pairs represent a wide range of flows, environmental conditions (e.g., laboratory and field, water and air), acquisition systems (e.g., laser power and camera bit-depth), and image characteristics.

The "Flume" and "Wave" images were obtained in laboratory experiments, using water as the seed medium. Both "Flume" experiments involved a relatively uniform flow field compared to the "Wave" experiments, in which strong shear was present. Both "Flume" and "Wave" images are of high quality, as flow conditions, particle seeding, and laser illumination were tuned for PIV. The "Ocean" images are in situ images, which were obtained near the Santa

Table 1 Technical specifications for each of the six experimental image pairs used to evaluate Intensity Capping

Image pair	Camera	Bits	Image size	Seed	I_0	σ_I
Flume_1	Kodak MegaPlus ES1.0	8	1030 × 992	GS	47/45	23/19
Wave_1	Kodak MegaPlus ES1.0	8	1030 × 992	GS	56/61	19/16
Air	Kodak MegaPlus ES1.0	8	1030 × 992	PG	22/22	35/35
Ocean	Cooke, CCD Sony ICX385	12	1040 × 1376	NT	65/64	23/25
Flume_2	Redlake MegaPlus ES4.0/E	12	2048 × 2048	GS	82/78	78/65
Wave_2	Redlake MegaPlus ES4.0/E	12	2048 × 2048	GS	64/68	56/66

I_0 is the grayscale median and σ_I is the grayscale standard deviation of the first and the second images in each pair. d_p is the diameter of the seed particles. The following seeding particles were used: *GS* hollow glass spheres made by Potters Industries ($d_p \approx 11$ μm); *PG* propylene glycol droplets ($d_p < 1$ μm); *NT* natural ocean seeding (suspended sediment, phytoplankton, and zooplankton) at approximately 40 m depth

Barbara Channel Islands, California. The ''Air'' image pair was acquired in the near-exit region of an air jet that injected seeded air into stagnant, unseeded air. Both ''Ocean'' and ''Air'' contain some regions of low seeding density due to the challenges associated with natural seeding (low particulate concentrations) and due to the un-seeded stagnant air, respectively. The last two columns of Table 1 provide the values of the grayscale median, I_0, and standard deviation, σ_I, of the original (uncapped) images for each experiment.

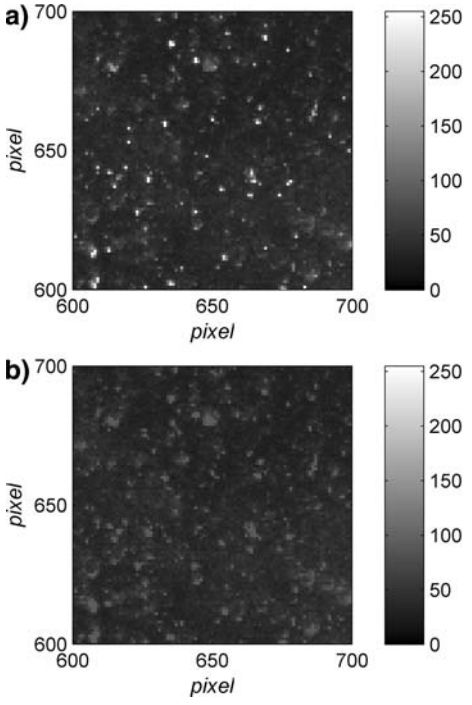

Fig. 2 Image intensity for an image (''Flume_1'') before (**a**) and after (**b**) the application of Intensity Capping. For clarity, only 1% of the (first) image area is shown. The upper limit used for the Intensity Capping was equal to $I_0 + 2{\cdot}\sigma_I$ (as in Fig. 1)

3.2 Results from experimental images

Figure 2 shows an example image (''Flume_1'', 1st image) before and after the application of Intensity Capping (~1% of the image area is shown). The upper limit grayscale intensity value used to cap the image was equal to $I_0 + 2{\cdot}\sigma_I$ (Fig. 1). A comparison of the two images shows that Intensity Capping eliminates the bright spots, while preserving the rest of the image. Note that the particles that produced the bright spots are still present in the capped image but appear with reduced intensity. Figure 3 shows the resulting unfiltered PIV results for both the original (uncapped) and capped image pairs (covering ~10% of the image area). Figure 3 demonstrates that Intensity Capping significantly reduces the number of outliers for this image pair.

Figure 4 shows cross-correlation maps for a single interrogation region from ''Flume_1''. These maps correspond to the center vector of the nine vectors shown in Fig. 4a (uncapped) and b (capped). In the uncapped case (Fig. 4a), two dominant correlation peaks are observed: the true peak associated with the net particle motion (left) and a spurious peak associated with the presence of bright spots (right). The application of Intensity Capping effectively reduces the height of the spurious peak and increases the height of the true cross-correlation coefficient peak (Fig. 4b). It should also be noted that the application of Intensity Capping acts to reduce intensity at particle centers (i.e., it makes particle intensity profiles look more like top-hat functions) and thus the width of the true correlation peak may broaden.

Figure 5 shows the Intensity Capping results at different values of n, calculated using MatPIV for each of the experimental image pairs. The results obtained using the other three codes (not shown) were qualitatively the same. Intensity Capping increases the percentage of valid velocity vectors for each of the image pairs, with no exception. As n declines from nearly

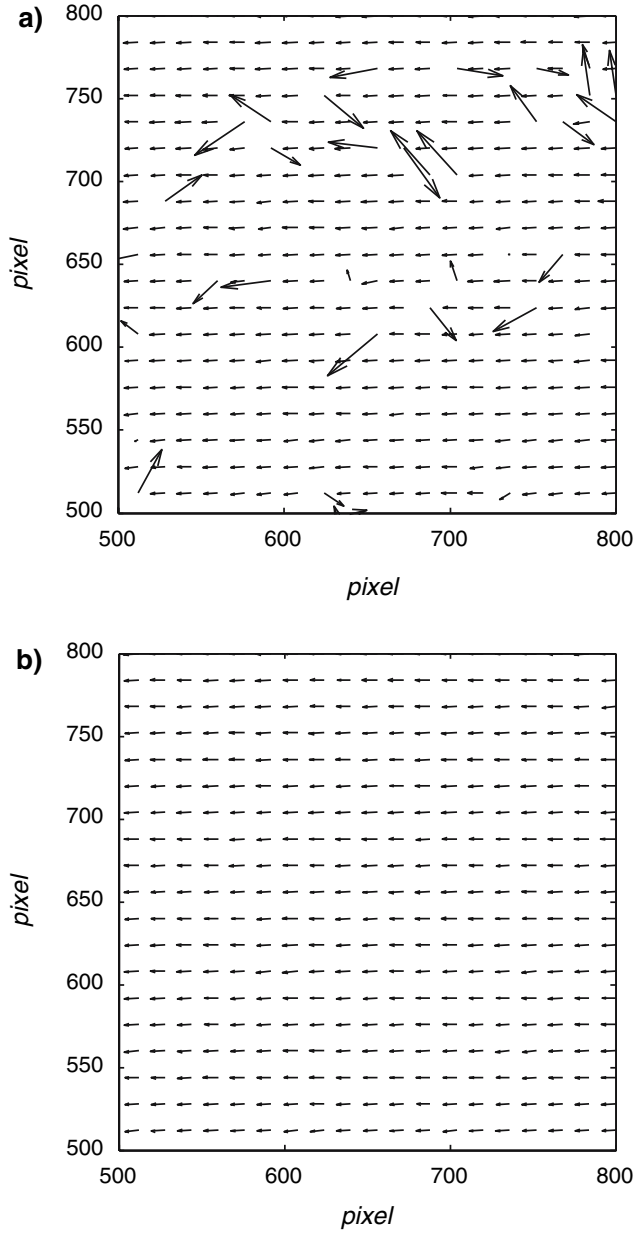

Fig. 3 Displacement vector field results for ''Flume_1'' with original (**a**) and capped (**b**) image pairs, corresponding to Figs. 2a and b, respectively. The mean horizontal displacement in (**b**) is 4.3 pixels. Note that only a small region of the velocity vector map is shown (~10%) so that individual vectors can be identified

uncapped values (e.g., $n \sim 11$ to 40), Intensity Capping exhibits improving performance, until a threshold value is achieved ($n \sim 0$ to 3) at which the PIV results rapidly degrade. Improved results are obtained for smaller n because bright spots are capped to a greater extent. At very low n values ($n \sim 0$), the image signal level (i.e., particle intensity) approaches the background noise and thus the results degrade. Figure 5 shows that a choice of $n =$ 0.5–3 yields the best PIV results. Further investigation of these experiments reveals that the optimal n value (based on the analysis of a subset of images) is typically valid for the entire set of images.

Table 2 summarizes the Intensity Capping results for combinations of the experimental image pairs and PIV codes. P_0 represents the percentage of valid vectors in the original (uncapped) images. P_{best} represents the highest percentage of valid vectors obtained using Intensity Capping. ''Improvement'' describes the relative change in the percentage of valid vectors due to Intensity Capping, i.e., $(P_{best} - P_0)/P_0 \times 100$. Lastly, n_{best} is the value of n used to generate P_{best}. The absolute percentage of valid vectors, P_0 and P_{best}, are dependent on the quality of the original images and PIV code performance and thus do not necessarily reflect the performance of Intensity Capping. For example, a camera defect left a thin, black (zero intensity) strip at the bottom of the ''Flume_1'', ''Air'', and ''Wave_1'' images. ''Flume_1'' and ''Air'' images were processed with the strip intact, while ''Wave_1'' was processed after the strip was removed. As a result, both P_0 and P_{best} are higher for ''Wave_1'' than for ''Flume_1'' and ''Air''. Therefore, it should be stressed that the relative improvement, not the absolute percentage of valid vectors (P_0 and P_{best}), is the relevant parameter for evaluating the performance of Intensity Capping.

The relative improvement in valid vectors due to Intensity Capping ranges from 1.6 to 11.1% (Table 2). The ''Ocean'' PIV results show the greatest improvement (11.1%) of all of the experiments (Table 2). The relatively narrow intensity histograms of the ''Ocean'' images ($\sigma_I = 23/25$ for 12-bit, Table 1) suggest that the uncapped images may be highly susceptible to PIV biases due to bright spots. Since the intensity variance in the images is small, bright spots make a large contribution to the cross-correlation and may thereby generate PIV outliers. This is exhibited in the relatively low absolute percentage of valid vectors ($P_0 = 86.1\%$). In the absence of bright spots (i.e., for the intensity capped images), the ''Ocean'' images yield a high percentage of valid vectors ($P_{best} = 96\%$).

The average improvement is somewhat higher for images that were generated by 12-bit cameras (i.e., ''Ocean'', ''Flume_2'', and ''Wave_2'') than for those generated by the 8-bit camera (i.e., ''Air'', ''Flume_1'', and ''Wave_1''). This result is expected since the grayscale intensity of a bright spot may be 16 times larger in a 12-bit camera than in an 8-bit camera. As the median and standard deviation of the grayscale intensities of the six image pairs are within the same order of magnitude (see Table 1), a bright spot in a

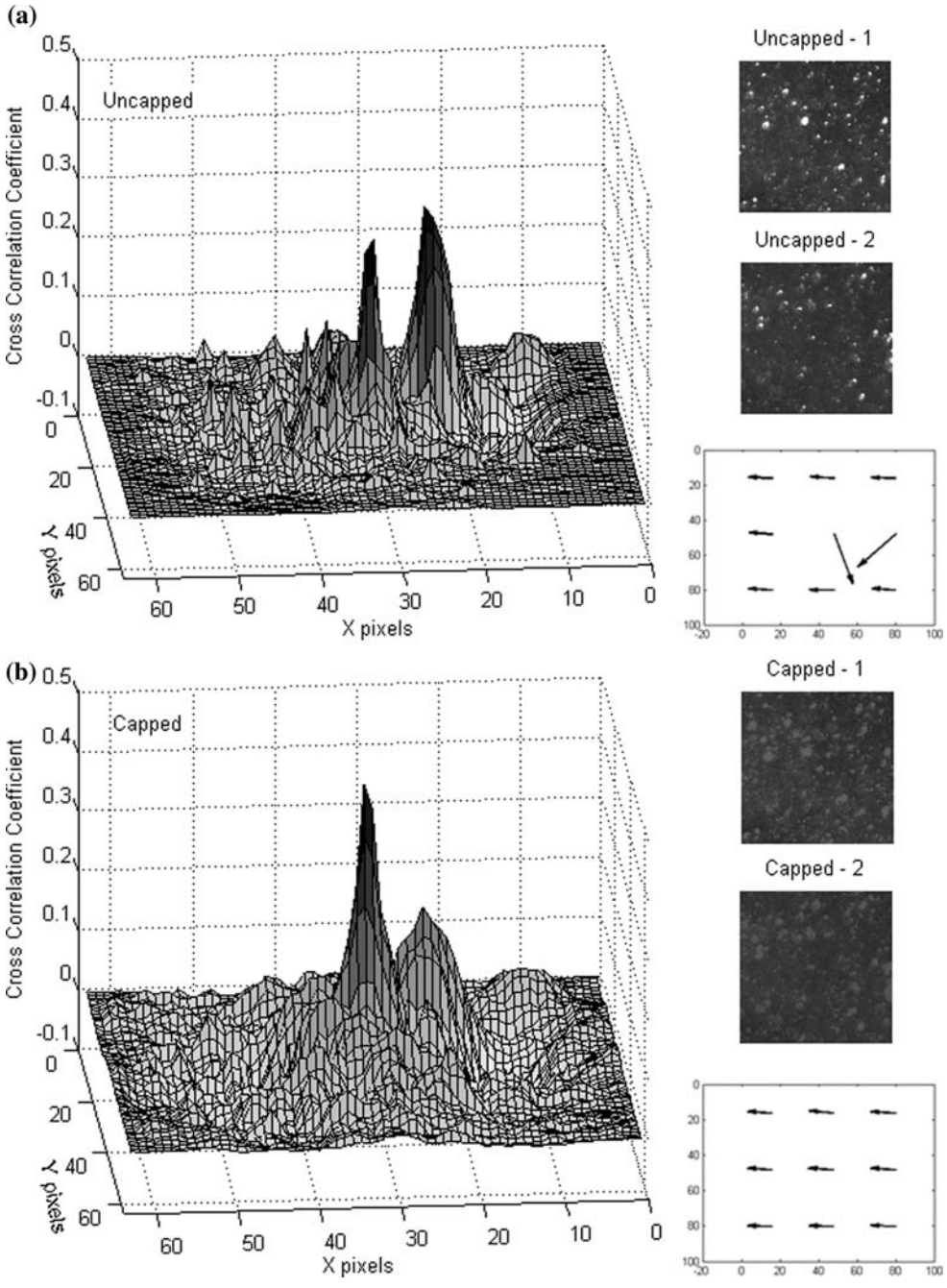

Fig. 4 Cross-correlation coefficient maps of one subwindow (32 × 32 pixels) in ''Flume_1'' before and after the application of Intensity Capping. The image subwindows and displacement results (shown in pixel coordinates) on the right cover a pixel area of $368 < x < 464$ and $752 < y < 848$. The cross-correlation coefficient maps correspond to the vector in the center of the displacement field. The results were obtained using MatPIV with two passes with no subwindow overlap

12-bit image is likely to have a greater influence on the cross-correlation than a bright spot in an 8-bit image.

Notably, Intensity Capping also improves PIV results for images that contain bright spots due to bad pixels on the CCD array. Damaged pixels (e.g., anomalously sensitive or saturated pixels) are common and their number may increase with camera age. The cross-correlation is likely to be dominated by damaged pixels that appear with the maximum possible value (e.g., 255 in 8-bit images). Images ''Flume_1'', ''Wave_1'' and ''Air'' have about 25 bad pixels (with a grayscale value of 255) that generate ~10 spurious vectors in each velocity field. Since the number of bad pixels in each interrogation window is relatively small, Intensity Capping reduces the influence of these stationary bad pixels and produces accurate velocity vectors in these regions. Note that when bad pixels appear in the same location in every image, other techniques such as background subtraction could be used to prevent spurious vectors. However, if bad pixels arise erratically in space or time, Intensity Capping is likely to be a superior solution.

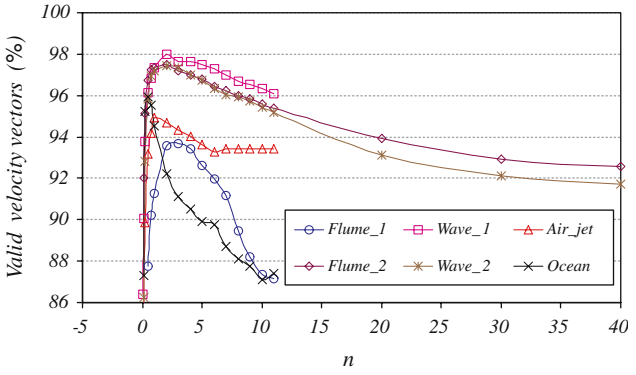

Fig. 5 The percentage of valid velocity vectors as a function of the number of standard deviations, n, used for the definition of the Intensity Capping upper limit. These results were obtained using MatPIV. The PIV results are optimal for n between 0 and 3. As n approaches zero (i.e., the upper limit nears the grayscale median), the number of valid vectors decreases sharply. In the opposite limit, as n becomes large, the percentage of valid vectors asymptotes to its uncapped value

In Table 2, the results obtained with three existing image-enhancement techniques (described in Sect. 2.3) are compared to those obtained with Intensity Capping. The level of improvement obtained using the MHE method is comparable, but slightly lower than that obtained by Intensity Capping for all of the experiments. It should be noted that for their particular images, Roth and Katz (2001) found that $x = 94\%$ gave the best results, while the best x values for our images varied between 40 and 65% for the 12-bit images and between 5 and 10% for the 8-bit images. For min/max, values cited in Table 2 represent the best results obtained among the four different tile sizes evaluated. These correspond to tile sizes of 9, 9, 25, 15, 9, and 9 for images ''Flume_1'', ''Wave_1'', ''Air'', ''Ocean'', ''Flume_2'' and ''Wave_2'', respectively. In most cases, the min/max technique significantly improves the results, but the percentage of valid vectors was lower than obtained using Intensity Capping. The application of min/max to the ''Air'' trial was one exception, in which a slight degradation resulted for all tile sizes. This may have been caused by the variable seeding density near the edges of the jet (see Sect. 3.1) The CLAHE function generally improves the results and performs slightly better than MHE, min/max and Intensity Capping. However, instead of improving the ''Ocean'' PIV results, CLAHE reduces the number of valid vectors from 86.1% in the original image pair to 82.5% in the enhanced images. It seems that the CLAHE algorithm is unable to effectively re-map the narrow intensity histogram of the ''Ocean'' images.

The relatively small modification to the images is another advantageous feature of Intensity Capping. While MHE, min/max, and CLAHE re-map the entire

Table 2 The results of the analysis of experimental images

	P_0	P_{best}	Improvement (%)	n_{best}	N_{capped} (%)	MHE	min/max	CLAHE
Flume_1								
MatPIV	87.2	93.7	7.5	3	1.8	93.3	92.4	94.0
VidPIV	88.8	94.9	6.8	3	1.8	–	–	95.5
URAPIV	86.5	93.0	7.5	3	1.8	–	–	94.3
TSI	89.5	94.6	5.8	2	3.0	–	–	95.2
Wave_1								
MatPIV	96.0	98.0	2.1	2	3.2	96.8	97.4	98.3
VidPIV	93.1	96.3	3.4	3	1.6	–	–	97.0
URAPIV	93.9	96.5	2.8	2	3.2	–	–	97.6
TSI	93.5	96.9	3.7	3	1.6	–	–	97.2
Air								
MatPIV	93.4	94.9	1.6	1	13	94.7	92.8	95.0
VidPIV	90.7	94.9	4.7	1	13	–	–	95.4
URAPIV	91.3	93.8	4.2	2	5.6	–	–	94.8
TSI	90.2	94.6	4.9	1	13	–	–	95.0
Ocean								
MatPIV	86.1	96.0	11.1	0.5	2.2	95.3	91.4	82.5
Flume_2								
MatPIV	92.3	97.5	5.6	2	2.4	97.0	97.3	98.7
Wave_2								
MatPIV	91.5	97.4	6.5	2	2.3	96.6	97.2	97.4

P_0 represents the percentage of valid vectors in the original (uncapped) images. P_{best} represents the percentage of valid vectors obtained using Intensity Capping. n_{best} is the number of standard deviations, n, used to generate P_{best}. N_{capped} is the percentage of pixels that were changed (capped) when P_{best} was obtained. N_{capped} represents the average between the first and second images of each image pair. For comparison, the last three columns show the percentage of valid vectors obtained following alternative image-enhancements techniques: MHE, min/max, and CLAHE

image and change the grayscale value of each pixel, Intensity Capping improves the PIV results by changing only a small fraction of the total number of pixels. Table 2 shows the percentage of pixels that were changed by Intensity Capping, N_{capped}, when P_{best} was obtained. Figure 6 shows that for all of the experimental image pairs, with the exception of the ''Air'' case, the number of changed pixels is less than 3.2% for $n = 2$, and less than 1.8% for $n = 3$. Thus, the best PIV results for each experiment are generally obtained while leaving at least 96.8% of the pixels unchanged. The relatively high values of N_{capped} for the ''Air'' image pair are related to the low median intensity value ($I_0 = 22$, Table 1) caused by the unseeded regions that appear on both sides of the air jet. Figure 6 also shows that the ''Ocean'' experiment, which shows the greatest improvement due to Intensity Capping, actually has the lowest fraction of pixels changed. Considered together, Figs. 5 and 6 indicate that a significant improvement in PIV results can be achieved with a very small modification to the images.

In addition to the aforementioned image-enhancement techniques, the performance of the symmetric phase only filtering (SPOF) algorithm modification (Wernet 2005) was also evaluated. The SPOF technique was selected for comparison because, like Intensity Capping, it is computationally inexpensive. We found that SPOF did not improve the PIV results for the set of experimental image pairs. While SPOF yields more accurate velocities for images containing DC background noise and low signal-to-noise ratio (SNR) cross-correlations (Wernet 2005), it appears that it is not well-suited to remedy displacement biases from bright spots characterized by high spatial frequency and high SNR cross-correlations. For PIV images containing both DC background noise and bright spots, we hypothesize that a combined approach involving both SPOF and Intensity Capping may be fruitful.

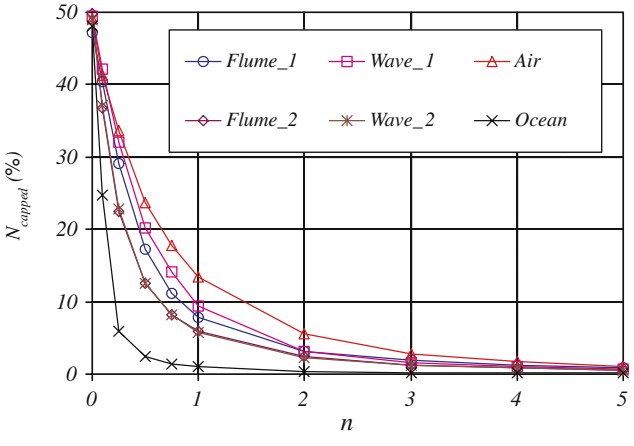

Fig. 6 The percentage of pixels that were changed by Intensity Capping, N_{capped}, as a function of the number of standard deviations, n, used to define the Intensity Capping upper limit

4 Evaluation of synthetic PIV images

4.1 Synthetic image generator

Simulated images have been used in many PIV analyses (Keane and Adrian 1992; Westerweel 1993; Cowen and Monismith 1997). Our image generator follows closely from the models described in Raffel et al. (1998) and Cowen and Monismith (1997).

Particles were randomly assigned a location within a simulated light sheet, using a uniform distribution. The particle seeding density was held fixed (except when explicitly varied), to an average of 15 particles/subwindow (32 pixels × 32 pixels). The particle locations in the first image were held constant for each set of trials to prevent variations in PIV results due to random particle placement. The particles were then subjected to a specified displacement prior to the generation of the second image.

A peak intensity, I_p, was specified for each particle located within the laser light sheet ($|Z| < 1/2\Delta Z_0$, where Z is each particle's cross-plane location and ΔZ_0 is the light sheet thickness). The light sheet profile was assumed to be Gaussian (Raffel et al. 1998), i.e.,

$$I_p(Z) = q \exp\left\{ \left[-Z^2\right] \Big/ \left[(1/8)\Delta Z_0^2\right] \right\}, \tag{7}$$

except where the effect of intensity distribution was specifically investigated. Here q is a user-specified maximum intensity within the light sheet. Since we specified the number of particles and distributed them uniformly within the light sheet, the thickness of the light sheet was arbitrary.

The image intensity, I, was then constructed by summing the contribution of scattered light from each particle, assuming a two-dimensional Gaussian intensity distribution about each particle center (Raffel et al. 1998):

$$I(x,y) = I_p \exp\left\{ \left[-(x-x_0)^2 - (y-y_0)^2\right] / \left[(1/8)d_p^2\right] \right\}, \tag{8}$$

where (x,y) are the image coordinates, (x_0, y_0) are the centers of each particle, I_p is the peak particle intensity (substituted from Eq. 7), and d_p is the particle diameter. As in Raffel et al. (1998), the magnification factor

between object plane and image plane was chosen to be unity. A diameter of 3 pixels was assigned to all particles. This diameter corresponds to the minimum rms error for PIV in the Monte Carlo simulations of Cowen and Monismith (1997). From the definition of I (Eq. 8), 95% of the scattered intensity is contained within the particle image diameter, d_p (Raffel et al. 1998). However, in our model, light was allowed to scatter up to three particle diameters, thus capturing nearly all of the scattered light from each particle.

Both ''ideal'' and ''realistic'' simulated images were generated and analyzed (Table 3). Ideal image trials (denoted I1–I5) were characterized as having no background image noise (Raffel et al. 1998) and optimum exposure (i.e., $q = 4{,}095$). Realistic simulated images (denoted R1–R3) included background noise and q was allowed to be sub-optimal. The background noise was specified as the sum of uniform background intensity and random intensity. To mimic our experimental images, the median and standard deviation of the realistic simulated images were both set to 50 and the shape of the intensity histograms were matched to our experimental image histograms. This was achieved by tuning the background noise and the peak particle intensity to the following values: background intensity, β, was set to 47.5; random intensity noise was specified by a Gaussian distribution, with values ranging from 0 to $\beta/5$; peak particle intensity, q, was set to 460. Note that background noise dominates the intensity statistics of PIV images, since particles occupy only a small fraction of the image area.

Lastly, all images were made to simulate 12-bit digital images by limiting intensity values to be between 0 and 4,095 and rounding all intensities to integer values. Intensity Capping was then applied in two ways. Ideal simulated images were capped at specific intensity values (ranging from 1 to 3,500); given that background noise was not present, the image intensity distributions were not well described by the median and standard deviation. Realistic simulated images were capped at specific n values (ranging from –0.1 to 11) in the same fashion as our experimental images.

4.2 Simulated particle motion

The imposed particle displacements between the first and second simulated PIV images were expressed as the superposition of uniform and variable components. Thus, each individual particle was assigned a displacement as follows:

$$d\boldsymbol{x} = \mathrm{d}\boldsymbol{x}_{\mathrm{uni}} + \mathrm{d}\boldsymbol{x}_{\mathrm{var}}, \tag{9}$$

where $\boldsymbol{x}$ indicates all three directional components of motion (x,y,z). The uniform contribution is given by a constant, $\mathrm{d}\boldsymbol{x}_{\mathrm{uni}}$ (set to 5 pixels in the x-direction for all trials), while the non-uniform contribution (e.g., due to turbulence or shear), is given by a variable displacement, $\mathrm{d}\boldsymbol{x}_{\mathrm{var}}$.

For turbulent flow trials, idealized two-dimensional (x,y) isotropic turbulence was imposed (see Table 3). Cross-plane, z-direction, particle motion effects were considered separately. To specify the level of turbulence, we generated turbulent displacements for each individual particle using a normal distribution with zero mean. The distribution of turbulent particle displacements was specified using the turbulence intensity, Tu, defined as rms $(\mathrm{d}\boldsymbol{x}_{\mathrm{var}})/\mathrm{d}\boldsymbol{x}_{\mathrm{uni}}$. For flows with shear, $\mathrm{d}\boldsymbol{x}_{\mathrm{var}}$ was prescribed as $\mathrm{d}x_{\mathrm{var}} = S_f \sin(2\pi\, y/32)$, where S_f specified the strength of the sheared displacement and y was the vertical image coordinate. Thus, we imposed vertical shear on the horizontal displacement such that the velocity profile was sinusoidal and periodic over each subwindow (32 pixels × 32 pixels). Cross-plane displacements were specified as a uniform displacement, $\mathrm{d}z_{\mathrm{uni}}$, with magnitudes varying from 0 to 50% of the laser light sheet thickness.

Table 3 Technical specifications for each of the simulated image trials used to evaluate Intensity Capping

Trial	Varied parameter	Light intensity distribution	Image noise	Flow conditions
I1	Turbulence intensity, Tu	Gaussian ($q = 4095$)	No	$\mathrm{d}x_{\mathrm{uni}} = 5$, $S_f = 0$
I2	Shear factor, S_f	Gaussian ($q = 4095$)	No	$\mathrm{d}x_{\mathrm{uni}} = 5$, Tu = 0
I3	Cross-plane displacement, $\%\Delta Z_0$	Gaussian ($q = 4095$)	No	$\mathrm{d}x_{\mathrm{uni}} = 5$, Tu = 0, $S_f = 0$
I4	Particle seeding density, n_{part}	Gaussian ($q = 4095$)	No	$\mathrm{d}x_{\mathrm{uni}} = 5$, Tu = 0.2, $S_f = 0$
I5	Peak particle intensity, I_p	Power law, $\beta = 300$, $C = 3{,}795$ (Eq. 10)	No	$\mathrm{d}x_{\mathrm{uni}} = 5$, Tu = 0.2, $S_f = 0$
R1	Turbulence intensity, Tu	Gaussian ($q = 460$)	Yes	$\mathrm{d}x_{\mathrm{uni}} = 5$, $S_f = 0$
R2	Shear factor, S_f	Gaussian ($q = 460$)	Yes	$\mathrm{d}x_{\mathrm{uni}} = 5$, Tu = 0
R3	Variable exposure, q	Gaussian (variable q)	Yes	$\mathrm{d}x_{\mathrm{uni}} = 5$, Tu = 0.2, $S_f = 0$

Trials I1– I5 consist of ''ideal'' simulated images, as they contain no background noise. Trials R1–R3 consist of ''realistic'' simulated images, as they match the general characteristics of the experimental images: they include background noise and they have sub-optimal peak particle intensity

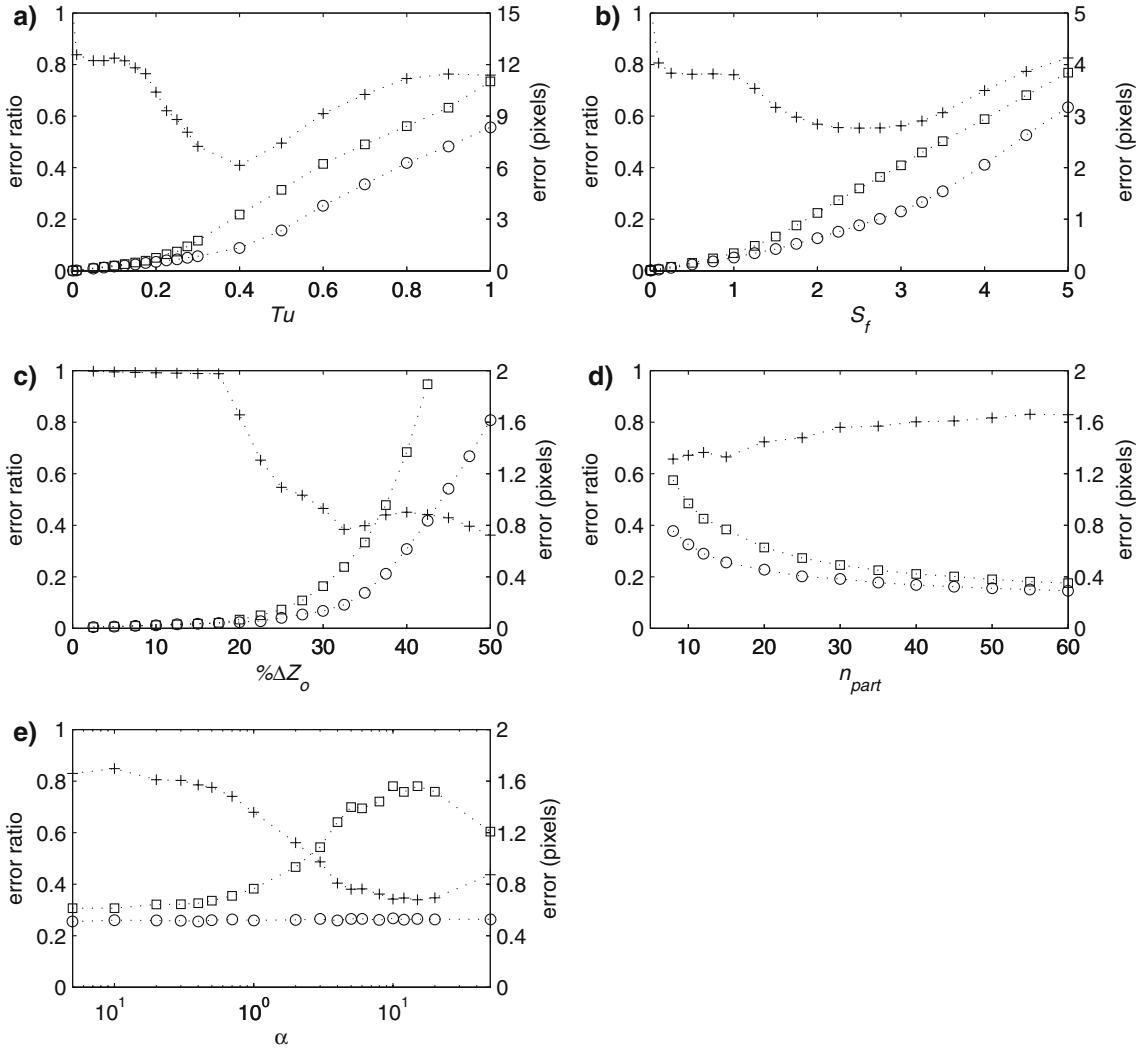

Fig. 7 Intensity Capping evaluation using ideal simulated images. *Squares* represent an uncapped rms error (in pixels); *circles* represent a capped rms error (in pixels); *plus signs* represent the ratio of capped error to uncapped error. Subfigures show the effects of varying: **a** turbulence intensity, *Tu* (Trial I1); **b** shear factor, S_f (Trial I2); **c** cross-plane motion, given as a percent of the light sheet thickness, $\%\Delta Z_0$ (Trial I3); **d** number of particles per PIV subwindow, n_{part} (Trial I4); and **e** distribution of peak particle intensity as determined by the parameter α (Trial I5, based on Eq. 10)

Using simulated images, it is possible to directly compare PIV-derived displacement calculations with the true mean particle displacement. Within each interrogation window, the true mean particle motion was computed as the mean displacement of all particles originating in the window. For each simulated trial, three replicates were performed to smooth variations in results due to the random initial particle location (in all trials) and the random displacement assignments in turbulence trials.

4.3 Results of synthetic image trials

To investigate the mechanisms responsible for the improvements observed with Intensity Capping in Sect. 3, we first consider the ideal simulated images (I1–I5 in Table 3; Fig. 7a–e).

Trials I1–I2 investigate the effect of individual particle motion relative to mean particle motion via turbulence and mean velocity shear. In such flows, the relative motion of bright spots to the mean particle motion may result in PIV errors. Figure 7a and b show that Intensity Capping reduces this displacement error for all values of turbulence intensity, Tu, and shear strength factor, S_f, considered. In turbulent flow, Intensity Capping yields the greatest improvement (about 60% reduction in rms displacement error from ~3.3 pixels to ~1.3 pixels) at around Tu = 0.4 (Fig. 7a). In sheared flow, the greatest improvement (~40% rms error reduction) is observed for levels of shear given by

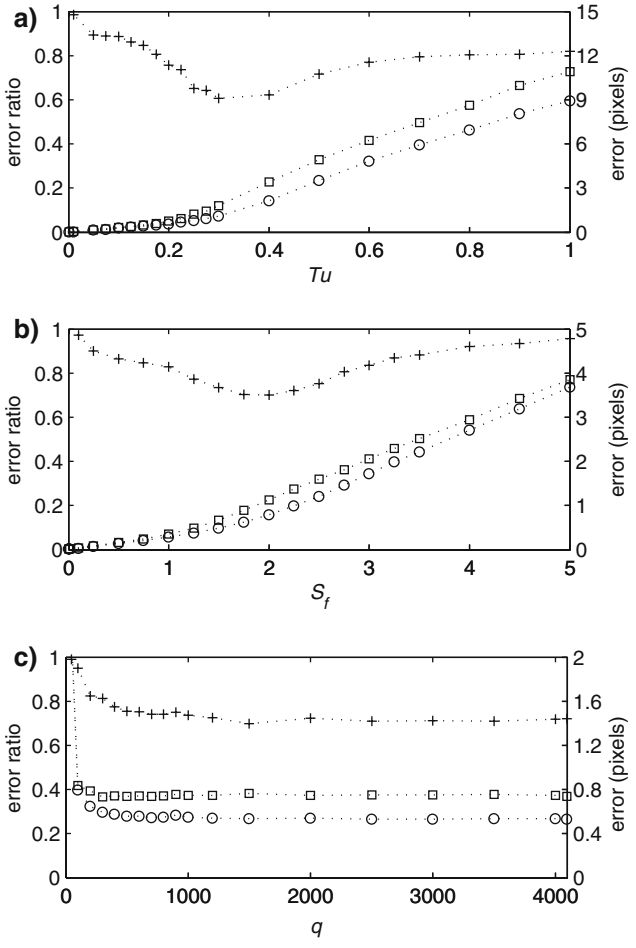

Fig. 8 Intensity Capping evaluation using realistic synthetic images. *Squares* represent an uncapped rms error (in pixels); *circles* represent a capped rms error (in pixels); *plus signs* represent the ratio of capped error to uncapped error. Subfigures show the effects of varying: **a** turbulence intensity, *Tu* (Trial R1); **b** shear factor, S_f (Trial R2); and **c** maximum light sheet intensity q (Trial R3)

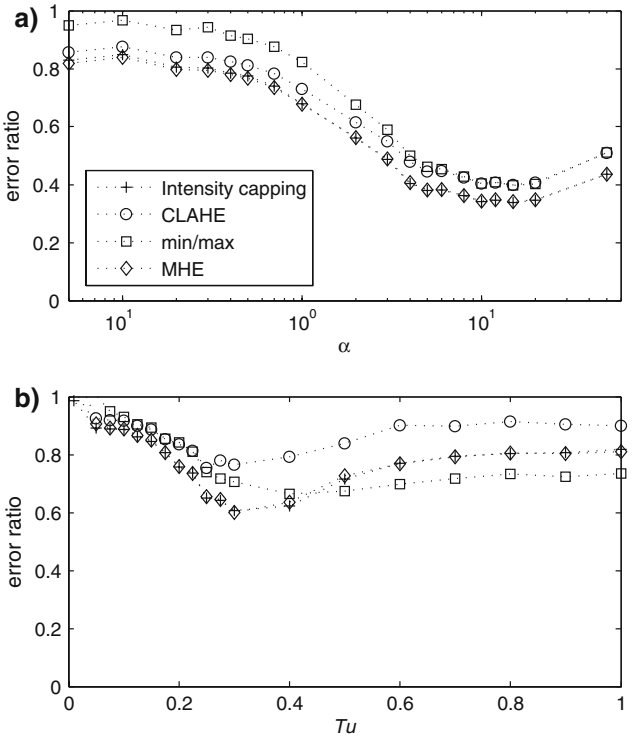

Fig. 9 Comparison of the image-enhancement techniques: Intensity Capping, CLAHE, min/max, and MHE. Subfigures show the effects of varying: **a** distribution of peak particle intensity, I_p, via the parameter α (Trial I5, based on Eq. 10); and **b** turbulence intensity, Tu (Trial I1). Note that in both subfigures, min/max results are shown for 5×5 pixel tile size, which produced the best results among the four tile sizes evaluated

S_f in the range ~2 to ~3 (Fig. 7b). Since turbulence and shear are present in many PIV experiments, Intensity Capping is a very attractive technique for reducing such PIV errors.

Cross-plane particle motion is common to many PIV experiments and may also result in PIV error due to particle pair loss and the generation of bright spots. For example, a particle may become a bright spot as it moves from the edge of the laser light sheet (where illumination is relatively low) to the light sheet center (a region of intense illumination). Particle pair loss may also cause bright spots to correlate with mismatched particles. Figure 7c (Trial I3) shows that Intensity Capping is effective at reducing PIV errors due to cross-plane particle motion, particularly for cross-plane displacements greater than 20% of the laser light sheet thickness.

The relative abundance of bright spots due to variations in particle seeding density also influences the error incurred by PIV. In Trial I4, the particle seeding density, n_{part}, is varied for a constant Tu = 0.2. When the seeding density is high, a bright spot has a small influence (or degradation potential) on the cross-correlation. Figure 7d shows that in this case, the uncapped PIV error and benefit of Intensity Capping are both relatively small. When the seeding is low, on the other hand, a bright spot may more readily bias the cross-correlation. In this case, the uncapped PIV error is high and Intensity Capping is particularly effective at reducing this error.

Trial I5 investigates the effectiveness of Intensity Capping for a variable proportion of bright spots in the images. For this trial, the peak particle intensity of each particle is specified by a power law,

$$I_p(k) = \beta + C[(k-1)/(N-1)]^{\alpha}, \tag{10}$$

where k refers to the kth particle, α is a user-specified exponent, β is the baseline peak particle intensity contribution, C is the bright spot contribution to peak

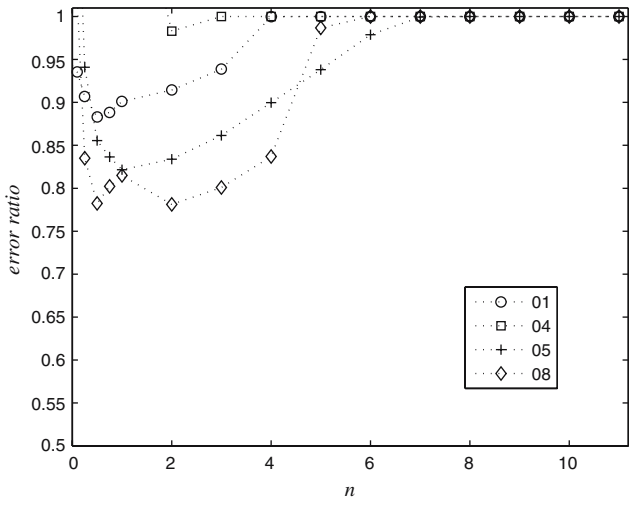

Fig. 10 Evaluation of Intensity Capping applied to standard, public domain, synthetic images provided by Okamoto et al. (2000). The error ratio, the ratio of capped rms displacement error and uncapped rms displacement error, is plotted as a function of n, the number of standard deviations used in the definition of the Intensity Capping upper limit. Results for four image pairs are shown: 'reference' (*circle*, 01); 'dense particle' (*square*, 04); 'sparse particle' (*plus sign*, 05); and 'large out-of-plane velocity' (*diamond*, 08)

particle intensity, and N is the total number of particles in the image. This model allows the user to control the proportion of bright spots in the image via the exponent parameter, α. For $\alpha = 0$, we recover the top-hat profile (i.e., no variation in I_p), $I_p = \beta + C$. For $\alpha = 1$, we have linear variation in I_p across all particles, ranging from β to $\beta + C$. For large α ($\alpha \gg 1$), we again reduce the variation in I_p, such that almost all particles have $I_p = \beta$, while a small number of particles are allowed to have higher intensities. Figure 7e shows that as α increases (and hence more bright particles are generated) for a constant Tu = 0.2, the PIV error increases and the improvement gained by Intensity Capping increases. For $\alpha > 20$, the uncapped PIV error becomes smaller because the variation in I_p actually declines, as almost all particles have a uniform peak intensity ($I_p = \beta$).

In order to evaluate the performance of Intensity Capping for more realistic image characteristics, three sets of realistic simulated images were analyzed (R1–R3 in Table 3). Trials R1–R2 demonstrate the performance of Intensity Capping for realistic simulated images with variable turbulence intensity and shear. Intensity Capping improves the results for the entire range of turbulence intensities and shear levels, with a peak improvement around Tu~0.3–0.4 and $S_f \sim 1.5$ – 2.5, respectively (Fig. 8a, b).

Trial R3 investigates the effect of variable signal-to-noise ratios by varying the peak particle intensity, q. Figure 8c reveals that the improvement due to Intensity Capping is consistently high when there is a large separation between the peak particle intensity and background noise ($q >$ ~1,000). For peak particle intensities closer to the noise intensity ($q <$ ~1,000), the improvement due to Intensity Capping attenuates, as the capping causes particle intensities to be comparable to the background noise.

The simulated images also allow for additional comparison of Intensity Capping with the other image-enhancement techniques: MHE, min/max, and CLAHE. Figure 9 shows the error ratio (ratio of rms displacement error for enhanced images to rms displacement error for unenhanced images) for Trial I5 and Trial R1.

Figure 9a (Trial I5) investigates the effects of bright spot frequency via the power law intensity model (Eq. 10). The four image-enhancement techniques follow the same general trend, with optimal performance occurring around $10 < \alpha < 20$, a range in which most particles have intensities near the baseline β and the remaining particles have elevated (bright) intensities ranging from β to $\beta + C$. For larger α ($\alpha > 20$), where almost all particles are of the baseline intensity β and few bright spots exist, the benefit of the enhancement techniques declines from optimal. The results of Intensity Capping and MHE are almost identical and perform slightly better than the CLAHE and min/max filters.

Figure 9b (Trial R1) investigates the effect of variable turbulence levels (the same conditions as shown in Fig. 8a). The results indicate that all four image-enhancement techniques reduce the PIV error (error ratio < 1) for typical turbulence levels (Tu < 0.3). The one exception to this observation occurs near Tu = 0 (i.e., Tu = 0.001 and 0.01) where the error in the PIV results from the unenhanced images is very small and thus the error ratio is a poor metric for performance. For very large levels of turbulence (Tu > 0.3), the techniques show a decline in performance. In general, Intensity Capping and MHE demonstrate superior performance for small Tu, while min/max is superior at relatively high Tu.

The performance of Intensity Capping was also tested using a set of standard, public domain, synthetic images (Fig. 10). Okamoto et al. (2000) produced synthetic PIV images based on three-dimensional LES simulations. For the current study, we analyzed four image pairs from a two-dimensional wall shear flow simulation (http://www.piv.vsj.or.jp/piv/image-e.html): a 'reference' image pair (named '01'); a 'dense particle' image pair (named '04', consisting of 10,000 particles compared to 4,000 particles in the 'reference' images);

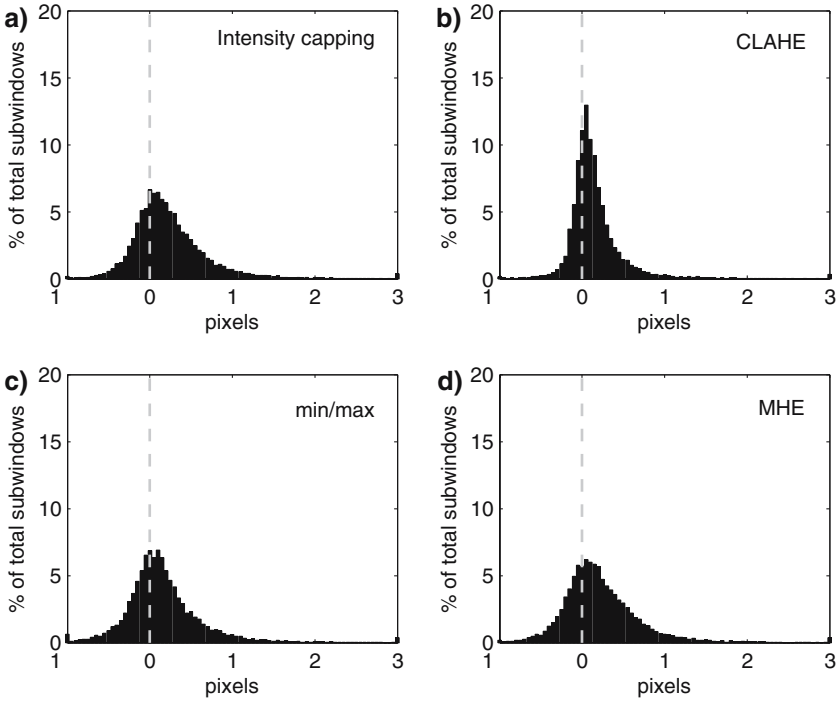

Fig. 11 Histograms of the displacement error improvement (pixels) due to image enhancement (positive values represent improvement and negative values represent degradation). The results of Intensity Capping (**a**) are compared with the results of the other techniques (**b–d**) for 0.2 turbulence intensity in Trial R1. The histogram counts were normalized by the total number of subwindows

a 'sparse particle' image pair (named '05', consisting of only 1,000 particles); and a 'large out-of-plane velocity' image pair (named '08'). In all these cases the first two images (out of four provided images) were chosen for the analysis. The images were capped with a range of n values and subsequently processed with MatPIV. The results from these standard images are consistent with the analysis of our own synthetic images: the improvement in PIV results due to Intensity Capping increases as the density of particles decreases. Also, Intensity Capping is particularly effective at reducing PIV errors for image pairs with out-of-plane particle motion.

While all of the previous examples demonstrate that Intensity Capping and the existing image-enhancement techniques effectively reduce rms displacement errors, the question remains as to whether these techniques may adversely affect some of the individual vectors (i.e., increase the error). To quantify this degradation effect to individual vectors, we plot histograms of the difference between PIV errors associated with the unenhanced images to those generated by analyzing enhanced images, for all velocity vectors. The difference between the PIV errors is defined such that positive values represent an improvement and negative values represent degradation.

For illustration, histograms are shown for Trial R1, with Tu = 0.2 and background noise present (Fig. 11). The percentage of vectors for which the PIV result was improved was 70% for Intensity Capping (Fig. 11a) and 68, 63, and 71% for MHE, min/max, and, CLAHE respectively (Fig. 11b–d). Thus, all of the techniques improve more vectors than they degrade. Additionally, all of the techniques reduce the rms displacement error for this case; the rms displacement errors are reduced from the 0.74 average pixel error associated with the original, unenhanced image (Fig. 8a), by 0.25, 0.24, 0.08, and 0.17 pixels for Intensity Capping, MHE, min/max, and CLAHE, respectively. For other trials, similar behavior is typically observed: more than 50% of the vectors are improved and the rms PIV error is reduced.

The source of the degradation of certain individual vectors for Intensity Capping could result from at least two sources: (1) the technique will tend to reduce the separation range between the background noise and the peak particle intensities, and (2) by capping the highest intensities, the correlation peak may broaden (e.g., see Fig. 4). The first effect is minimized by selecting the appropriate level of capping (i.e., n) such that the particle intensity remains above the background noise and an improvement in the PIV results is observed. To investigate the second effect, we consider the case from Trial I1 when Tu = 0 (i.e., $d\boldsymbol{x}_{\mathrm{var}} = 0$) and the images are capped at an extreme value of 1 (i.e., the resulting capped images are binary). Given that there is no background noise and no relative particle motion ($d\boldsymbol{x}_{\mathrm{var}} = 0$) for this case, the resulting error will simply result from the ability of the PIV code to find the correlation peak. The rms displacement error was

0.008 for the original, uncapped case and 0.010 pixels for the binary, capped case. We conclude that even for this extreme binary capping, where the correlation peak would presumably be broadest, the added error can effectively be neglected (representing only a 0.002 pixel error in a 5 pixel mean displacement).

5 Conclusions

The results of this paper indicate that Intensity Capping offers an efficient solution to the common PIV problem of spurious vectors generated by bright spots that move relative to the mean particle motion. Intensity Capping is implemented prior to PIV analysis and therefore any PIV code, open source or commercial, can be used without modification.

In all of the cases considered, Intensity Capping shows excellent performance. For the set of experimental images considered, Intensity Capping always yields PIV results with a reduced percentage of spurious vectors, as measured by a local consistency filter. Our analysis shows that a choice of $n = 0.5$–3 generally yielded the best results. However, since an optimal n depends on the particular image noise characteristics, its value should be confirmed for each new set of experiments. For a large set of simulated images, Intensity Capping reduces the rms particle displacement error for all parameter ranges considered. Analysis of Intensity Capping in the context of existing image-enhancement techniques shows that it typically performs better or comparably for a wide range of image and flow conditions.

An attractive feature of Intensity Capping is that it has a minor effect on the measurement error. For example, the degradation in pixel displacement accuracy due to extreme binary capping was found to be negligible. Intensity Capping also only modifies a relatively small fraction of the total image pixels relative to other image-enhancement techniques. The image modification only affects those pixels having exceedingly high intensities. MHE, min/max, and CLAHE remap the entire image, including the background noise; background noise may be amplified and may thereby lead to PIV errors. Intensity Capping is different in that it only alters the highest intensity particles (i.e., not the background noise), and thus it avoids noise amplification. Furthermore, the removal of the peak intensity values by Intensity Capping has a minor effect on displacement error since the particle image location information is contained in the intensity gradients that separate the particles from the background. Intensity Capping has less influence on these gradients than other enhancement techniques relying on spatial filtering. It is also important to note that the pixels affected by Intensity Capping still contribute to the displacement calculation. Bright spots may represent particle pairs that are important to the result of the cross-correlation. Intensity Capping does not eliminate the contribution of these bright pixels, but simply reduces their relative weight and as a result, the cross-correlation better represents the majority of the particle pairs.

It is important to place the proposed Intensity Capping procedure in the context of previous studies of camera bit-depth and PIV image enhancement. Willert (1996) studied the effect of bit-depth on PIV, using scanned photographs. The PIV images were obtained by scanning particle photographs at different bit-depths (1-bit to 8-bit). Willert (1996) found that bit-depth played a minor role in the final measurement uncertainty. For example, PIV results based on binary images consist of only 10–20% more errors than those based on 8-bit images (Willert 1996). This finding and the performance of Intensity Capping indicate that high quality PIV results can be obtained from images of relatively narrow dynamic intensity range. However, it should be noted that Intensity Capping is different from this scanning procedure. In the scanning procedure, the intensity values are mapped to a new bit-depth, but bright spots remain. Intensity Capping, on the other hand, removes bright spots without changing the bit-depth.

The preceding analysis has focused strictly on the performance enhancement offered by the various image-enhancement techniques, while ignoring the important issue of computational cost. Intensity Capping adds only one simple step to the PIV analysis process and is therefore very efficient. We evaluated the computation time required to enhance a 12-bit 1024×1024 pixel image and found that CLAHE (tiles of 8×8 pixels), MHE, and min/max (9×9 pixel tiles) respectively took 12, 273, and 1,068 times longer to enhance images than Intensity Capping. It is important to note that efficient algorithms can help improve the speed of tile by tile techniques (Roth and Katz 2001). However, given that CLAHE includes an optimized algorithm and MHE is implemented using a single tile, we conclude that Intensity Capping should generally be more computationally efficient than the other techniques. PIV studies that involve complex flow problems (e.g., turbulent flows) often require a large number of realizations. When thousands of image pairs are processed, it is desirable to minimize computation time associated with the image-enhancement procedures. The low computational cost of Intensity

Capping makes it a particularly attractive technique for large PIV data sets.

Finally, the proposed Intensity Capping technique could be further developed. Non-uniform (tile by tile) intensity capping may be more effective when large spatial variations in the image background exist. To achieve optimal results, it may then be necessary to perform intensity capping within discrete tiles using local, rather than global, intensity statistics. Intensity capping could also be developed into an error detection tool. The user could analyze an image pair with and without Intensity Capping. The results from Intensity Capping may then be used as a filter to reject spurious vectors in the PIV results from the uncapped images. This may be particularly useful when a user wishes to process unenhanced images, but still seeks to validate and filter the results.

Acknowledgments The authors are grateful for the discussions with J. Rosman, J. Koseff, and S. Monismith and the technical help provided by R. Gurka and R. Rosenzweig. The authors extend special thanks to M. Wernet for implementing his SPOF technique. The authors would like to acknowledge contributions to the Ocean PIV project by J. Jaffe, P. Roberts, F. Simonet, P. Franks, S. Monismith, C. Troy, and A. Horner-Devine. Support for Ocean PIV was provided by NSF grant OCE-0220213. R. Lowe acknowledges support from NSF grant OCE-0453117.

References

Cowen EA, Monismith SG (1997) A hybrid digital particle tracking velocimetry technique. Exp Fluids 22:199–211

Dellenback PA, Macharivilakathu J, Pierce SR (2000) Contrast-enhancement techniques for particle-image velocimetry. Appl Optics 39(32):5978–5990

Fore LB, Tung AT, Buchanan JR, Welch JW (2005) Nonlinear temporal filtering of time-resolved digital particle image velocimetry data. Exp Fluids 39:22–31

Gurka R (1999) Dynamics of a flexible tube in the turbulent gas flow of a twin fluid atomizer. M.Sc. thesis, Technion, Israel

Gurka R, Liberzon A, Hefetz D, Rubinstein D, Shavit U (1999) Computation of Pressure Distribution Using PIV Velocity Data. In: Third international workshop on particle image velocimetry, Santa Barbara, California, pp. 671–6, September 16–18, 1999

Keane RD, Adrian RJ (1992) Theory of cross-correlation analysis of PIV images. Appl Sci Res 49:191–215

Lowe RJ (2005) The effect of surface waves on mass and momentum transfer processes in shallow coral reef systems. PhD thesis, Stanford University

Okamoto K, Nishio S, Saga T, Kobayashi T (2000) Standard images for particle-image velocimetry. Meas Sci Technol 11:685–691

Raffel M, Willert C, Kompenhans J (1998) Particle image velocimetry: a practical guide. Springer, Berlin Heidelberg New York

Rosenzweig R (2005) The macroscopic velocity profile near permeable interfaces: piv measurements, numerical simulations, and an analytical solution of the laminar problem. M.Sc. thesis, Technion, Israel

Roth GI, Katz J (2001) Five techniques for increasing the speed and accuracy of PIV interrogation. Meas Sci Technol 12:238–245

Shavit U, Moltchanov S, Agnon Y (2003) Particles resuspension in waves using visualization and PIV measurements—coherence and intermittency. Int J Multiph Flow 29:1183–1192

Sveen KJ (2004) An introduction to MatPIV v. 1.6.1, eprint series, Dept. of Math. University of Oslo, ''Mechanics and Applied Mathematics'', NO. 2 ISSN 0809–4403, August, 2004

Wernet MP (2005) Symmetric phase only filtering: a new paradigm for DPIV Data Processing. Meas Sci Technol 16:601–618

Westerweel J (1993) Digital Particle Image Velocimetry. Theory and Practice, PhD Thesis, Delft University of Technology, The Netherlands

Willert C (1996) The fully digital evaluation of photographic PIV recordings. Appl Sci Res 56(2–3):79–102